Journal of Power Sources 243 (2013) 95–101

Contents lists available at SciVerse ScienceDirect

Journal of Power Sources

journal homepage: www.elsevier.com/locate/jpowsour

Enhanced hydrogen oxidation activity and H_2S tolerance of Ni-infiltrated ceria solid oxide fuel cell anodes

Behzad Mirfakhraei, Scott Paulson, Venkataraman Thangadurai, Viola Birss*

Chemistry Department, University of Calgary, 2500 University Drive NW, Calgary, Alberta, Canada T2N 1N4

HIGHLIGHTS

- Catalytic amounts (≤3 wt.%) of Ni were infiltrated into porous GDC anodes.
- Ni-infiltration significantly enhanced the rate of the H_2 oxidation reaction.
- Far less S poisoning was observed for Ni-infiltrated GDC anodes in 10 ppm H_2S.
- Ni-infiltrated GDC anodes exhibit improved long-term stability in 10 ppm H_2S.

ARTICLE INFO

Article history:
Received 27 February 2013
Received in revised form
8 May 2013
Accepted 28 May 2013
Available online 6 June 2013

Keywords:
Solid oxide fuel cell
Ceria anode
Sulfur poisoning
Ni catalyst
Impedance spectroscopy
H_2 oxidation

ABSTRACT

The effect of Ni infiltration into porous Gd-doped ceria (GDC) anodes on their H_2 oxidation performance, with and without added 10 ppm H_2S, is reported here. Porous GDC anodes (ca. 10 μm thick) were deposited on yttria stabilized zirconia (YSZ) supports and then infiltrated with catalytic amounts of a Ni nitrate solution, followed by electrochemical testing in a 3-electrode half-cell setup at 500–800 °C. Infiltration of 3 wt.% Ni into the porous GDC anode lowered the polarization resistance by up to 85%, affecting mainly the low frequency impedance arc. When exposed to 10 ppm H_2S, the Ni-infiltrated anodes exhibited a ca. 5 times higher tolerance toward sulfur poisoning compared to GDC anodes alone, also showing excellent long-term stability in 10 ppm H_2S. In the presence of H_2S, it is proposed that Ni, likely distributed as a nanophase, helps to maintain a clean GDC surface at the Ni/GDC interface at which the H_2 oxidation reaction takes place. In turn, the GDC will readily supply oxygen anions to the adjacent Ni surfaces, thus helping to remove adsorbed sulfur.

1. Introduction

Solid oxide fuel cells (SOFCs) are electrochemical devices that efficiently and cleanly convert the chemical energy of fuels directly to electricity and heat. High efficiency, fuel flexibility, low emissions, and modularity are the key advantages of combined heat and power SOFC systems that are helping to drive this technology forward [1]. Owing to their high working temperature (600–800 °C), SOFCs are capable of using natural gas, diesel, etc. as a fuel. However, common SOFC anode materials, such as nickel–yttria-stabilized zirconia (Ni–YSZ), suffer from several disadvantages, such as coking in hydrocarbon fuels [2], poisoning even at low levels of H_2S [3,4], and redox instability with accidental air exposure [5].

To overcome these problems, ceria and doped-ceria mixed ion and electron conductors (MIECs) have been extensively studied as anodes, due to their high catalytic activity and their ability to use hydrocarbon fuels without coking [6–9]. As recently proposed by Shishkin and Ziegler [10] and experimentally proven by Chueh et al. [11] and Nakamura et al. [12], ceria alone is catalytically active for H_2 oxidation. The use of ceria-based MIEC anodes increases the number of active sites without the need for a three phase boundary, as in the case of metal–oxide composites, thus helping to lower the polarization resistance (R_p). For example, it has been shown that increasing the ceria layer thickness from 7 to 45 μm linearly decreased the R_p value due to the associated higher catalytic surface area [12].

However, it has also been reported that Gd-doped ceria suffers from sulfur poisoning when exposed to 10 ppm H_2S [13] and several studies have been carried out to understand and overcome this problem [14–20]. Ni–GDC composite anodes (with a Ni content above the electron conduction percolation limit) have shown

* Corresponding author.
E-mail address: birss@ucalgary.ca (V. Birss).

0378-7753/$ – see front matter © 2013 Elsevier B.V. All rights reserved.
http://dx.doi.org/10.1016/j.jpowsour.2013.05.150

particularly promising performance [21–23], illustrating better hydrogen oxidation reaction (HOR, reaction (1)) kinetics and H_2S tolerance compared to conventional Ni–YSZ anodes [24].

$$H_2\ (g) + O^{2-}_{(GDC)} \rightarrow H_2O\ (g) + 2e^-_{(GDC)} \quad (1)$$

Another issue is redox instability, caused by the extensive expansion of Ni when it is converted to NiO [25], which can degrade the Ni–GDC anode. This can be minimized by using only catalytic amounts of Ni (below the percolation limit of conductivity). Primdahl et al. have demonstrated that a catalytic amount (0.8 wt.%) of Ni infiltrated into a porous GDC structure significantly decreased R_p [26,27]. Liu et al. have also shown a positive effect of the addition of 4 wt.% Ni to a $La_{0.8}Sr_{0.2}Cr_{0.8}Mn_{0.2}O_{3-\delta}$–GDC composite anode when operated in either H_2 or C_3H_8 [28]. However, the effect of catalytic amounts of Ni on the sulfur tolerance of GDC anodes has not been investigated as yet.

In the present study, the effect of Ni infiltration into a porous GDC anode layer on both its HOR activity and sulfur tolerance has been studied using a 3-electrode half-cell set-up at between 500 and 800 °C. It is shown that Ni infiltration significantly improves the HOR activity, affecting mainly the low frequency arc in open circuit impedance measurements. Ni infiltration (≤3%) into ceria also significantly decreases the extent of H_2S poisoning, showing only a ca. 5% increase in R_p at 800 °C, compared to a ca. 40% activity loss for GDC alone, while also greatly improving the anode stability over longer time periods.

2. Experimental procedure

2.1. Cell fabrication

A thin film of $Gd_{0.1}Ce_{0.9}O_{1.95}$ (GDC, d_{50} = 0.3–0.5 μm, Fuel Cell Materials Ltd.), mixed with a terpinol-based carrier, was applied to one side of a dense 1 cm × 1 cm × 0.5 mm Ceraflex YSZ (8 mol.% yttria stabilized zirconia) sheet to form circular (either 0.33 or 0.50 cm^2) working electrodes (WE). A symmetrical counter electrode (CE) and a small reference electrode (RE) were painted on the other side of the YSZ sheet using a similar terpinol-based paste. After drying at 120 °C, the cell was calcined at 1200 or 1250 °C for 4 h to form a porous, 10–20 μm thick GDC electrode. The cells that were fired at 1250 °C reached a stable baseline more rapidly in constant voltage or current experiments than those fired at 1200 °C, while the other properties of these cells remained the same. A microliter pipette was used to infiltrate 0.1 M $Ni(NO_3)_2.6H_2O$ in ethanol into the porous GDC layer, with the solution being seen to fully absorb into the anode structure. As the Ni map (EDX, Fig. 1c) also showed a uniform distribution of Ni throughout the anode microstructure, it was concluded that the Ni content of the anode was indeed 3 wt.%.

Au paste (C 5729, Heraeus Inc., Germany) normally served as the WE, CE and RE current collectors, with Pt paste (LP A88-11S, Heraeus Inc., Germany) sometime used for comparison. Au mesh was then attached to the WE, while Pt mesh was used to contact the RE and CE. The entire cell was then heated to 800 °C at 3 °C min^{-1} in 5 ml min^{-1} N_2 + 20 ml min^{-1} H_2 (3% H_2O), followed by cell testing.

2.2. Electrochemical studies

Electrochemical experiments were carried out in a half-cell set-up at 100 °C intervals between 500 and 800 °C using a mass flow controller adjusted gas mixture of 20 ml min^{-1} H_2 (3% H_2O) and 5 ml min^{-1} of either N_2 or 52 ppm H_2S in N_2 (to generate 10 ppm H_2S). Electrochemical impedance spectroscopy (EIS), constant current (galvanostatic), constant potential (potentiostatic), and open circuit potential (OCP) measurements were carried out using a Solartron 1287/1255 potentiostat/galvanostat/impedance analyzer. OCP EIS analyses (0 V bias, ±10 mV rms, 10^{-2} to 10^5 Hz) were first carried out from high to low frequency and then low to high to verify that the cell was stable and that the EIS data were reproducible. Constant potential experiments were carried out at a 100 mV anodic overpotential, while the applied currents were selected so that the measured anode overpotential was also roughly 100 mV. To confirm that the results obtained from constant potential and constant current experiments were in agreement, especially in the case of H_2S exposure, some samples were tested using both methods back to back.

2.3. Structural characterization

The microstructure and composition of both the as-prepared and long-term tested samples were determined using a Philips XL 30 scanning electron microscope (SEM) with energy dispersive X-ray analysis (EDX) capabilities (Microscopy and Imaging Facility, University of Calgary). Fractured samples were used to determine the porosity, inter-particle connectivity, and the overall microstructure of the working electrode film. The distribution of Ni in the GDC porous structure was established during cross-sectional analysis by wavelength dispersive spectrometry (WDS), using a JEOL JXA-8200 electron microprobe (University of Calgary, Laboratory for Electron Microprobe Analysis).

3. Results and discussion

3.1. Anode microstructure

A highly porous SOFC anode structure is desired in order to facilitate the transport of fuel to electrochemically active sites and to remove the products from the anode pores. Good connectivity between the anode particles is also necessary in order to provide ionic and electronic conductivity across the electrode layer, which, in turn, enhances the anode activity and decreases its polarization resistance (R_p). To achieve this type of microstructure for porous GDC electrodes, often with varying Gd dopant contents, sintering temperatures of 1100–1350 °C have typically been used in the literature [12,19,27]. It is known that, as the sintering temperature increases, the active surface area decreases, resulting in a higher *R*p value. Primdahl and Liu [27] reported a low *R*p for a 40 mol.% Gd-doped ceria that was sintered at 1100 °C. In the present study, sintering temperatures of 1200 and 1250 °C were used to enhance the cell stability and to establish a stable baseline for the H_2S poisoning studies.

Fig. 1a shows the microstructure of a typical screen-printed, porous GDC electrode, fired at 1250 °C for 4 h and then infiltrated using 40 μl of a 0.1 M Ni nitrate solution, giving about 3 wt.% Ni after reduction. Fig. 1b shows the structure of a similar electrode, but after more than 60 days of electrochemical testing at 500–800 °C (mainly at 700 and 800 °C) in a reducing atmosphere. Both SEM images show that the GDC particles have good inter-particle connectivity and that the GDC layer has sufficient porosity for unimpeded gas transport. The Ni infiltrate could not be resolved in these SEM images, indicating that Ni is present in the form of nanoparticles, similar to what was observed by Tucker et al. after Ni nitrate infiltration into porous YSZ [29]. However, WDS elemental mapping of Ni, using an electron microprobe (Fig. 1c), shows a uniform distribution of Ni within the porous GDC structure.

After long term (ca. 60 days) testing (Fig. 1b, inset), the GDC particles have sharper edges and appear to be somewhat more sintered as compared to the as-prepared sample (Fig. 1a, inset).

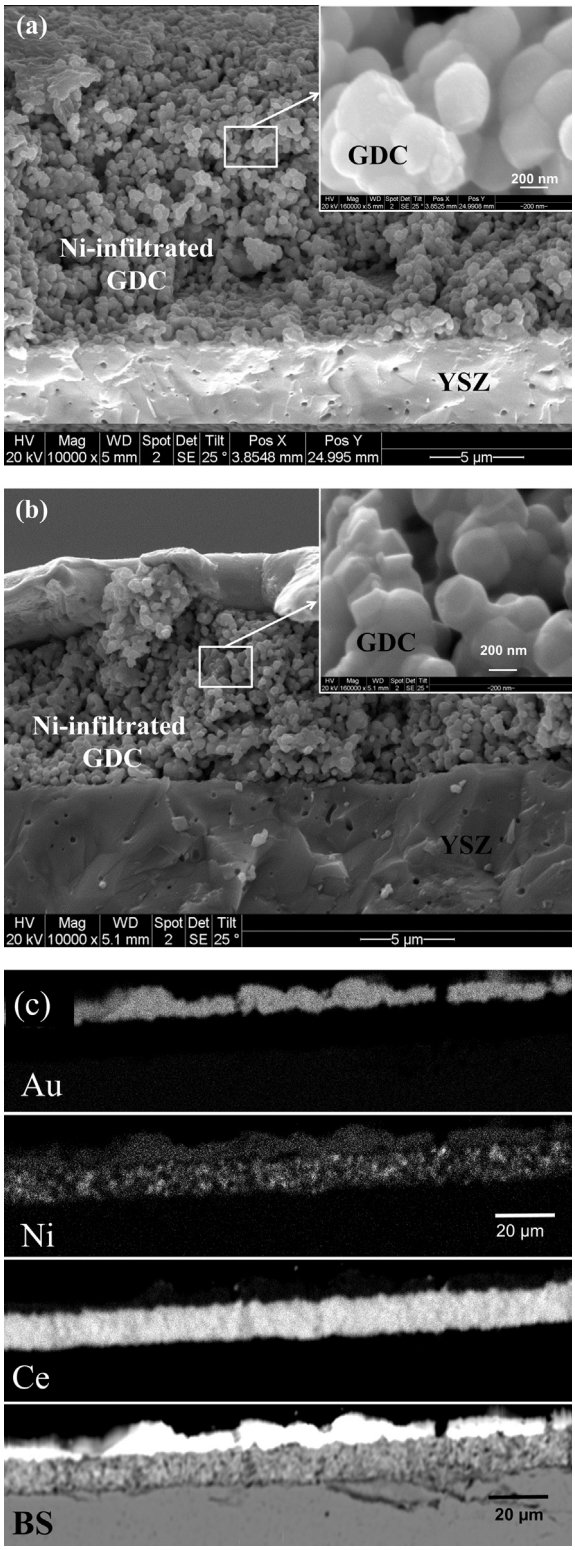

Fig. 1. SEM cross-sectional images of porous 3 wt.% Ni-infiltrated GDC on YSZ (fired at 1250 °C for 4 h) after (a) reduction in (H_2 + 3% H_2O) at 800 °C for 12 h before electrochemical testing, (b) after electrochemically testing for 60 days in 20 ml min^{-1} (H_2 + 3% H_2O) + 5 ml min^{-1} N_2, and (c) electron microprobe WDS maps of Au, Ni and Ce along with a backscattered (BS) image of the sample shown in (b), revealing a uniform distribution of Ni in the infiltrated anode layer.

However, the GDC–YSZ interface (Fig. 1b and c) remains in good condition, even after long term experimentation, and the Au current collector is still very well-connected to the anode.

3.2. Comparison of performance of GDC and Ni-infiltrated GDC

3.2.1. EIS study of the hydrogen oxidation reaction (HOR) at open circuit conditions

Fig. 2(a–d) shows the very beneficial effect (significantly lower polarization resistance) of Ni infiltration into the porous GDC layer on the open circuit EIS response at various temperatures, seen to affect primarily the low frequency arc. Although the impedance data could sometimes be fitted reasonably well with a two RC equivalent circuit, most of the EIS data showed the presence of three RC equivalent circuit, with an intermediate summit frequency of 1–100 Hz. Thus, a three RC equivalent circuit (Fig. 3) was used to fit all of the EIS data in this paper. Primdahl et al. attributed the low frequency arc (summit frequency of ca. 0.1 Hz) to the slow dissociative adsorption of hydrogen on the GDC surface [26,27], giving a large capacitance of 0.3–0.9 F cm^{-2} [27], while Liu et al. also supported this idea in a similar study on the $La_{0.8}Sr_{0.2}Cr_{0.8}Mn_{0.2}O_{3-\delta}$–GDC system [28]. The high frequency arc, with a summit frequency of ca. 1 kHz, has not been studied in great depth, although it has been postulated to reflect a combination of a charge transfer step during the hydrogen oxidation reaction and the transport of oxide ions in the GDC and/or at the GDC/electrolyte interface [26,27]. The origin of the intermediate arc remains uncertain at this time.

Most importantly, after Ni infiltration, the total R_p decreased by 85, 80, 80 and 90% at 500, 600, 700 and 800 °C (Fig. 2(a–d)), respectively, versus the non-infiltrated sample. Consistent with this, the literature has shown that the infiltration of 0.8 wt.% Ni into a porous GDC40 anode (40 mol.% Gd-doped ceria) significantly enhances the cell performance, especially by decreasing the resistance of the low frequency arc by about 80% (measurements were done at 850 °C in H_2 + 3% H_2O) [26,27]. Infiltration with 3 wt.% Ni, equivalent to 1.8 vol.% Ni, is insufficient to form a well interconnected (percolating) Ni network, which has been reported to require a minimum of 9 vol.% Ni [30,31]. The Ni present in the anodes studied in Fig. 2 is therefore serving only to catalyze the H_2 oxidation reaction.

In order to determine if the low frequency arc (arc 3) is affected by a gas diffusion process, as suggested by Primdahl et al. [26,27] and Aravind et al. [32], the effect of the substitution of N_2 with He in the fuel flow on the EIS spectra of the Ni-infiltrated sample was examined, as shown in Fig. 3. For this sample, which was fired at 1250 °C for 4 h, a high frequency arc (arc 1) with a 1 kHz summit frequency appears, while at lower frequencies, two arcs are present, categorized as the intermediate (arc 2) and low frequency arcs. Although some of the GDC or Ni-infiltrated GDC anodes did not show arc 2, the equivalent circuit $R_\Omega(R_L L)(RQ)_1(RQ)_2(RQ)_3$ (Fig. 3, inset) was consistently used to fit all of the impedance data, with the inductive time constant representing the low frequency inductor, seen in Fig. 3. In the equivalent circuit, R_Ω and R_L combine to give the series resistance ($R_s = R_\Omega + R_L$), while L, Q, n, and R are the inductance, constant phase element (CPE), CPE exponent, and resistance, respectively.

As shown in Fig. 3, only the low frequency arc (arc 3, summit frequency of 0.1 Hz) is affected by the He/N_2 gas exchange, confirming that it reflects a mass transport controlled process that becomes faster (lower R_p) when N_2, a larger molecule, is replaced by the smaller He. This is expected, as the diffusion coefficient of the H_2/He gas mixture is higher than the H_2/N_2 gas mixture at a constant mixing ratio [33]. This revealed that the resistance of the low frequency arc (arc 3) decreased by ca. 20% when N_2 was

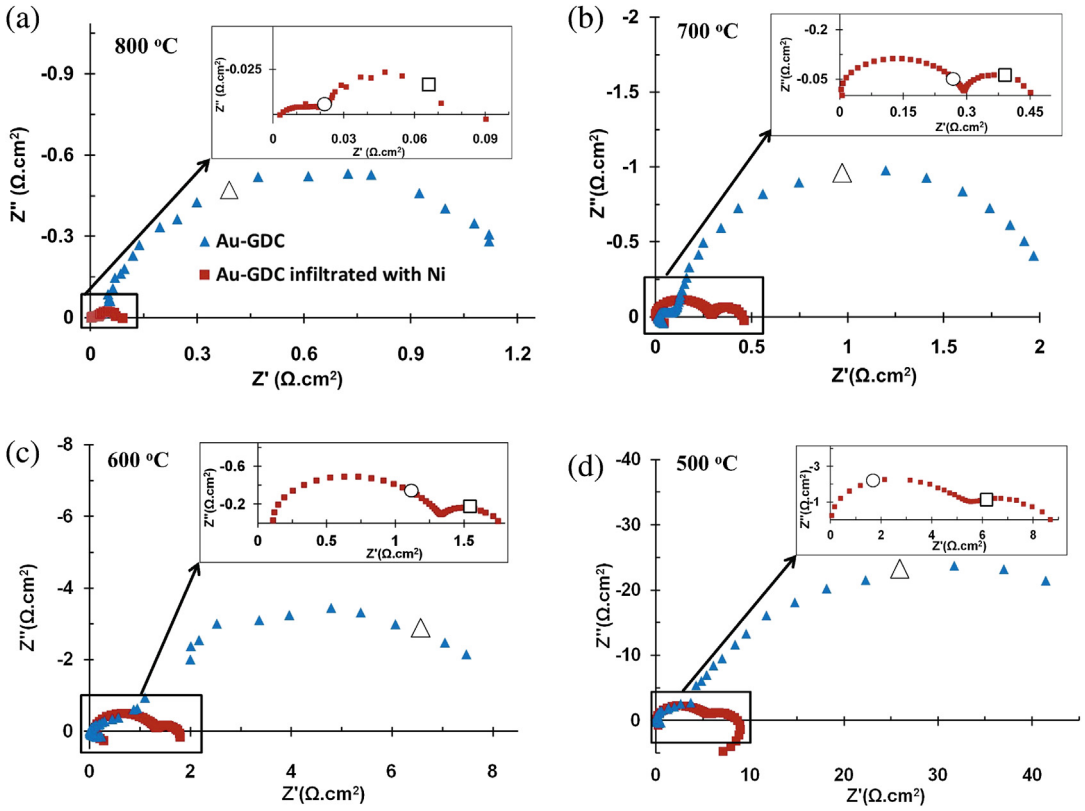

Fig. 2. Effect of 2 wt.% Ni infiltration on the impedance spectra of a porous GDC anode (fired at 1200 °C for 4 h) at 800–500 °C (a–d), with expanded views of the Ni–GDC data shown in the insets, at a gas flow of 20 ml min^{-1} (H_2 + 3% H_2O) + 5 ml min^{-1} N_2. For easier comparison, the series resistance has been subtracted. (○), (□) and (Δ) represent 100, 1 and 0.1 Hz, respectively.

switched to He. This demonstrates that there is a contribution from bulk mass transport to the low frequency impedance response, thus also affecting the total polarization resistance, R_p. Interestingly, a similar impact on arc 3 is also seen in the H_2S poisoning studies, as discussed below.

3.2.2. EIS study of H_2S poisoning and recovery at open circuit conditions

The OCP EIS responses of the GDC and the Ni-infiltrated GDC anodes to 10 ppm H_2S in a 20 ml min^{-1} (H_2 + 3% H_2O) + 5 ml min^{-1} N_2 or (N_2 + 52 ppm H_2S) gas mixture at 700 °C are compared in Fig. 4. The parameters obtained by fitting the EIS data to the $R_\Omega(R_L L)(RQ)_1(RQ)_2(RQ)_3$ circuit are shown in Table 1. After exposure to 10 ppm H_2S in the fuel stream, the total R_p of the GDC anode is seen (Fig. 4) to increase by ca. 50% in 1 h, from 1.95 Ω cm^2 to 2.93 Ω cm^2, which is much greater than the increase in R_p of the Ni-infiltrated GDC anode (ca. 5.5% after 24 h, from 0.87 Ω cm^2 to 0.92 Ω cm^2). Importantly, H_2S exposure affects only the low frequency arc, adding about 55 and 25% to its resistance for the GDC and Ni-infiltrated GDC anodes, respectively (R_3, Table 1). This can be compared to the ca. 200% increase in R_p of a conventional Ni–YSZ anode when 8 ppm H_2S was introduced at 800 °C [4]. Table 1 confirms that the high and intermediate frequency arcs remain essentially unchanged by H_2S exposure.

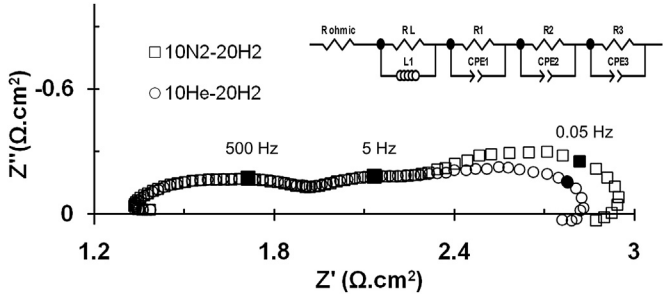

Fig. 3. Impedance spectra of a 3 wt.% Ni-infiltrated GDC anode (fired at 1250 °C for 4 h) in 20 ml min^{-1} (H_2 + 3% H_2O) + 10 ml min^{-1} N_2 (□) or 10 ml min^{-1} He (○), both at 700 °C. The equivalent circuit used for fitting is shown in the inset.

Fig. 4 also shows the EIS response after removal of the H_2S from the fuel stream. While the GDC sample shows about 90% recovery (Table 1), the Ni-infiltrated sample recovers almost completely back to its original R_p value. During the recovery, just the low frequency arc changes and the higher frequency arcs (arcs 1 and 2) remain constant.

Comparing Figs. 2 and 4, it can be seen that Ni infiltration enhances the same low frequency process that H_2S poisoning slows down. As is noted in the literature [26,27] and mentioned earlier, Ni infiltration is assumed to enhance the rate of hydrogen adsorption and thus the propensity for subsequent H atom spillover onto the ceria surface. Fig. 4 therefore suggests that H_2S occupies the H adsorption sites on Ni, as expected [4], thus lowering the number of available sites for the HOR and resulting in an increase in the low frequency arc resistance. Although 10 ppm H_2S should not affect the rate of gas diffusion in the porous electrode, it will slow down the H surface adsorption process, which would also affect the low frequency arc (arc 3).

At a constant temperature and H_2S partial pressure, the sulfur coverage is expected to be higher on metallic surfaces, such as Ni, compared to on most oxide surfaces, such as ceria

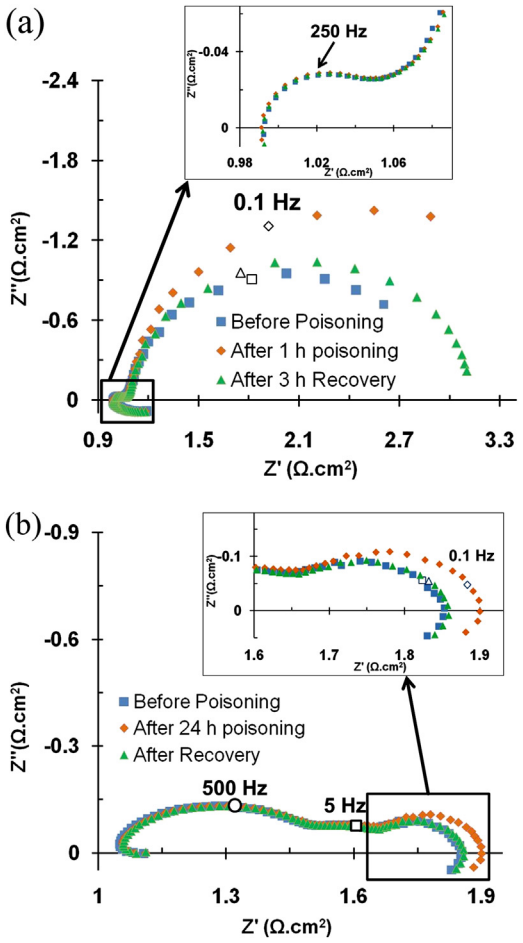

Fig. 4. Effect of 10 ppm H_2S on the OCP impedance spectra at 700 °C of (a) a GDC anode, with the high frequency arc shown in the inset, and (b) 3 wt.% Ni-infiltrated GDC anode, with the low frequency arc shown in the inset, before (■) and after (◆) exposure to H_2S and after recovery (▲).

[16]. Thus, in the early stages of sulfur poisoning, H_2S will be adsorbed primarily on Ni rather than on ceria. Ceria is a well-known oxygen donor [10] that can readily supply oxygen ions to the surface of the adjacent Ni, oxidizing the adsorbed sulfur on Ni (near the Ni/ceria interface) and keeping it clean for further adsorption of H_2. Consequently, the extent of sulfur poisoning of Ni-infiltrated GDC should be lower compared to what is seen at the GDC anode.

In parallel to this, dissociative adsorption of hydrogen will occur more rapidly on Ni as compared to on GDC [27] and thus hydrogen spillover onto the GDC surface can occur. As it is clear that the oxidation of hydrogen can take place quite readily on GDC [10,34], GDC will provide the needed oxygen anions and also serve to pass the electrons to the current collector. These synergistic processes may explain the ca. 10 times lower extent of sulfur poisoning of Ni-infiltrated GDC compared to GDC alone (5.5% compared to 50% R_p increase, respectively) at 700 °C, as shown in Table 1. The poisoning by H_2S of Ni–GDC is also lower than what has been reported for conventional Ni–YSZ composite anodes [4].

3.2.3. H_2S poisoning and recovery under polarized conditions

The effect of H_2S exposure on Ni-infiltrated GDC and single-phase GDC was also examined under anodic polarization conditions at 700 °C. Fig. 5a and c shows the raw data obtained from a potentiostatic study of H_2S poisoning at a 100 mV anodic overpotential. As is shown in equation (2), the R_p values reported in Fig. 5b and d, were calculated by subtracting R_s (the EIS-determined series resistance) from the total resistance, obtained, as a function of time, by dividing the applied anode overpotential (η) by the measured current (i) (Fig. 5a and c).

$$R_p = R_{tot} - R_s, \quad \text{where } R_{tot} = V/i = \eta/i \tag{2}$$

For this calculation, it was assumed that the 100 mV overpotential was in the linear (low field) part of the Butler–Volmer equation [35], where polarization activation does not affect the results. In fact, the percent H_2S poisoning values, obtained from back to back open circuit EIS and polarized i/t studies (not shown here), were very similar, suggesting that this assumption is valid. A similar percentage of H_2S poisoning was also obtained from galvanostatic experiments, in which the current needed to generate the same overpotential (~100 mV) was applied.

As is shown in Fig. 5, both GDC and Ni-infiltrated GDC exhibit poisoning upon exposure to H_2S in the gas stream. The R_p value of the Ni-infiltrated GDC anode (Fig. 5c and d) reaches a plateau after only ca. 2 h (inset, Fig. 5c) and does not increase further, while after H_2S removal, R_p recovers back to its initial value. In contrast, R_p of the GDC anode increases by roughly 5 times more than the Ni-infiltrated GDC with H_2S exposure and does not recover back to its initial value when H_2S is removed. These poisoning experiments were stopped after only a few hours of H_2S exposure at each temperature in order to protect the anodes from any irreversible damage that might occur. The increase in H_2S poisoning with decreasing temperature follows the expected increase of sulfur coverage on Ni [36] and an increased reactivity with ceria [16]. At this time, the temperature dependence of the H_2S poisoning data is not sufficiently resolved to generate an Arrhenius trend.

Table 1
Effect of 10 ppm H_2S[a] on the EIS circuit elements[b] of GDC and Ni-infiltrated GDC anodes at 700 °C (OCP EIS data shown in Fig. 4).

Anode	Condition	R_s[c] (Ω cm²)	R_1 (Ω cm²)	CPE_1 (mF cm^{-2})	n_1	R_2 (Ω cm²)	CPE_2 (F cm^{-2})	n_2	R_3 (Ω cm²)	CPE_3 (F cm^{-2})	n_3
GDC	No H_2S	1.08	0.05	10	1[d]	0.06	0.74	0.71	1.84	0.87	1[d]
	1 h H_2S	1.08	0.05	10	1[d]	0.06	0.83	0.68	2.82	0.89	1[d]
	After H_2S	1.09	0.05	10	1[d]	0.06	0.71	0.76	2.02	0.92	1[d]
Ni–GDC	No H_2S	1.01	0.50	9.5	0.62	0.15	0.41	0.74	0.22	4.2	0.83
	24 h H_2S	1.02	0.50	9.9	0.62	0.15	0.40	0.75	0.27	3.7	0.83
	After H_2S	1.02	0.50	9.6	0.62	0.14	0.40	0.74	0.22	4.0	0.83

[a] Gas flow: 20 ml min^{-1} (H_2 + 3% H_2O) + 5 ml min^{-1} N_2 or (N_2 + 53 ppm H_2S).
[b] Circuit elements obtained by fitting the impedance data of Fig. 4 to the $R_\Omega(R_L L)(RQ)_1(RQ)_2(RQ)_3$ equivalent circuit.
[c] $R_s = R_\Omega + R_L$, as done by Nakamura et al. [12].
[d] The n-values were very close to unity and thus they were fixed at 1 to enhance the accuracy of EIS circuit fitting.

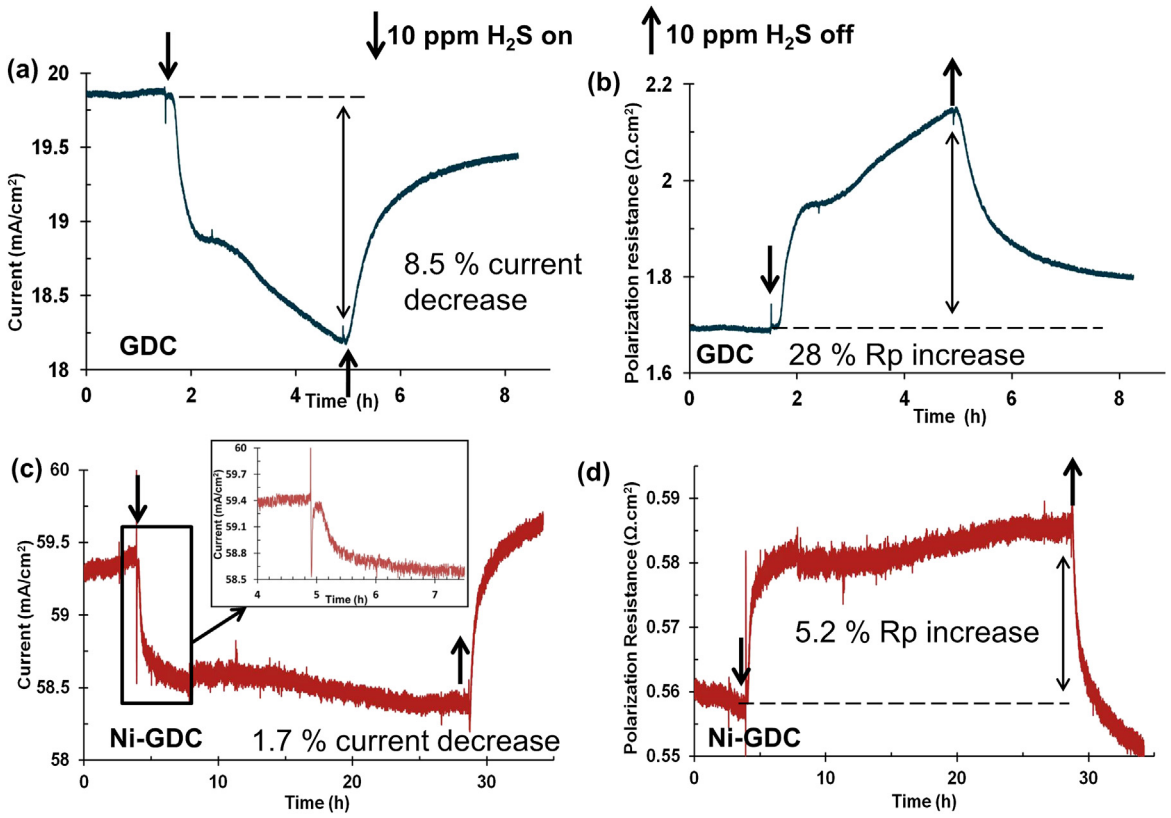

Fig. 5. Polarized 3-electrode half-cell H_2S poisoning data (a and c) and calculated polarization resistance (b and d) for GDC and Ni–GDC anodes, respectively. The inset (in part c), shows the early stage of the Ni–GDC sample H_2S poisoning. The data were acquired at a 100 mV anodic overpotential, all at 700 °C and a gas flow of 20 ml min^{-1} (H_2 + 3% H_2O) + 5 ml min^{-1} N_2 or (N_2 + 53 ppm H_2S).

As is shown in Fig. 6, the porous GDC anodes suffer from a larger R_p increase compared to the Ni-infiltrated GDC samples at all temperatures when they are exposed to H_2S at a 100 mV anodic overpotential. The average increase in R_p after H_2S poisoning is about 6, 9 and 15% for the Ni-infiltrated samples at 800, 700 and 600 °C, respectively, while the GDC samples poison roughly five times more (39, 48 and 72%, respectively) all at 100 mV. As the temperature decreases, a higher sulfur coverage on Ni [36] and ceria is expected, thus causing a higher degree of poisoning, as is seen in Fig. 6.

As is shown in Fig. 5c and d, the Ni-infiltrated anodes exhibit very good performance stability (for 24 h) in 10 ppm H_2S after the initially observed sulfur poisoning, in contrast to the GDC anodes, which poison continuously with time (Fig. 5a and b). Fig. 7 shows the results of a longer (3 days) exposure study of a 3 wt.% Ni-infiltrated GDC anode to 10 ppm H_2S, again at 100 mV anodic overpotential. After rapid 6.5% poisoning, the cell performed robustly for 3 days and then recovered fully to its original performance upon H_2S removal.

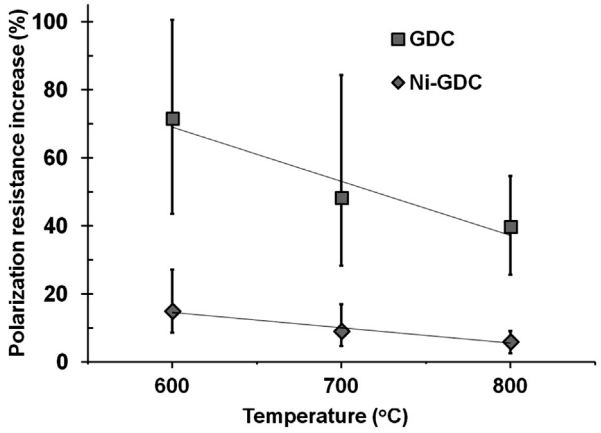

Fig. 6. Effect of 10 ppm H_2S on the polarization resistance of GDC (■) and Ni-infiltrated GDC (◆) anodes at 600–800 °C. Lines are drawn as a guide to the eye. Each data point is the average of the measurements made with a minimum of three different cells, using both galvanostatic and potentiostatic results at an anode overpotential of 100 mV.

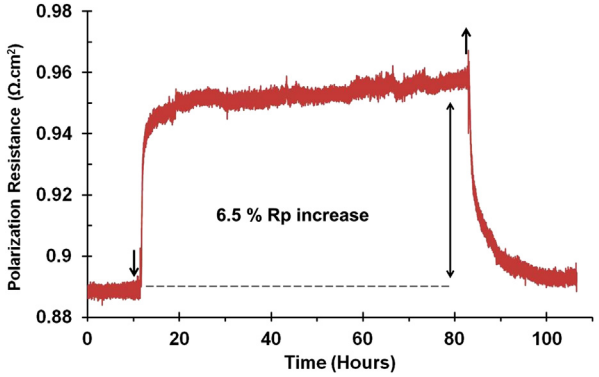

Fig. 7. Long term (72 h) exposure of 3 wt.% Ni-infiltrated GDC to 10 ppm H_2S at 100 mV anodic polarization at 700 °C and a gas flow of 20 ml min^{-1} (H_2 + 3% H_2O) + 5 ml min^{-1} N_2 or (N_2 + 53 ppm H_2S).

4. Conclusions

This work is aimed at understanding the effect of Ni infiltration on the performance of a porous GDC anode. Open circuit impedance and polarized electrochemical studies were used to show that both the hydrogen oxidation reaction activity and the H_2S tolerance of GDC were considerably enhanced when a catalytic amount of Ni (up to 3 wt.%) was infiltrated into the porous GDC anode structure. Both the hydrogen oxidation reaction activity and the H_2S tolerance of GDC were found to be considerably enhanced when a catalytic amount of Ni (up to 3 wt.%) was infiltrated into the porous GDC structure. The significantly smaller R_p (which decreased by ca. 85% at 800 °C with Ni infiltration) arises mainly from a decrease in the low frequency arc, which was linked to the rate of H_2 adsorption. Subsequent H spillover from Ni onto the GDC surface creates an additional reaction pathway for the hydrogen oxidation reaction, which is faster compared to direct H_2 adsorption on GDC alone. This beneficial rate enhancement is observed at all operating temperatures investigated here (500–800 °C).

Ni-infiltrated GDC anodes also show considerably improved stability compared to GDC alone when exposed to 10 ppm H_2S. There are two possible explanations for this effect. First, it is possible that, in the presence of Ni, the sulfur coverage on GDC (especially in the region of the Ni/GDC interface) will be lower than for GDC alone, as Ni may serve as a "sulfur adsorber" or "sulfur getter", removing it from the nearby GDC surface. It is also possible that the significantly larger amount of steam that is produced during H_2 oxidation when Ni is present (related to the much smaller polarization resistance) helps to remove adsorbed sulfur from both Ni and the nearby GDC [37], lowering the overall extent of sulfur poisoning caused by H_2S (reaction (3)).

$$2H_2O\,(g) + S\,(a) \rightarrow SO_2\,(g) + Ni + 2H_2 \quad (3)$$

Both of these hypotheses could be applicable, especially as Ni is distributed in a nanostructured form on the surface of GDC, thus greatly increasing the Ni/GDC interfacial length. This, in turn, enhances the bi-functional effects described above.

Acknowledgments

The authors gratefully acknowledge the financial support from the Institute for Sustainable Energy, Environment and Economy (ISEEE) at the University of Calgary and the NSERC Solid Oxide Fuel Cell Canada Strategic Research Network from the Natural Science and Engineering Research Council of Canada (NSERC) and other sponsors listed at www.sofccanada.com. We are also grateful for NSERC PGSD scholarship support of BM.

References

[1] S. Singhal, High Temperature Solid Oxide Fuel Cells, first ed., Elsevier, Cornwall, 2003.
[2] H. He, J.M. Hill, Applied Catalysis A: General 317 (2007) 284–292.
[3] Z. Cheng, J.-H. Wang, Y. Choi, L. Yang, M.C. Lin, M. Liu, Energy & Environmental Science 4 (2011) 4380–4409.
[4] S. Zha, Z. Cheng, M. Liu, Journal of The Electrochemical Society 154 (2007) B201–B206.
[5] J.L. Young, V. Vedharathinam, V.I. Birss, ECS Transactions 35 (2011) 1697–1706.
[6] D.K. Niakolas, J.P. Ouweltjes, G. Rietveld, V. Dracopoulos, S.G. Neophytides, International Journal of Hydrogen Energy 35 (2010) 7898–7904.
[7] S. Park, J.M. Vohs, R.J. Gorte, Nature 404 (2000) 265–267.
[8] E.P. Murray, T. Tsai, S.A. Barnett, Nature 400 (1999) 649–651.
[9] T.-J. Huang, C.-H. Wang, Chemical Engineering Journal 132 (2007) 97–103.
[10] M. Shishkin, T. Ziegler, The Journal of Physical Chemistry C 114 (2010) 21411–21416.
[11] W.C. Chueh, Y. Hao, W. Jung, S.M. Haile, Nature Materials 11 (2011) 155–161.
[12] T. Nakamura, K. Yashiro, A. Kaimai, T. Otake, K. Sato, T. Kawada, J. Mizusaki, Journal of The Electrochemical Society 155 (2008) B1244–B1250.
[13] B. Mirfakhraei, V.I. Birss, V. Thangadurai, S. Paulson, K.E. Bere, F. Gitzhofer, ECS Transactions 35 (2011) 1727–1734.
[14] R.M. Ferrizz, R.J. Gorte, J.M. Vohs, Applied Catalysis B: Environmental 43 (2003) 273–280.
[15] M. Gong, X. Liu, J. Trembly, C. Johnson, Journal of Power Sources 168 (2007) 289–298.
[16] P. Lohsoontorn, D.J.L. Brett, N.P. Brandon, Journal of Power Sources 175 (2008) 60–67.
[17] P. Lohsoontorn, D.J.L. Brett, N.P. Brandon, Journal of Power Sources 183 (2008) 232–239.
[18] G.J. Offer, J. Mermelstein, E. Brightman, N.P. Brandon, Journal of the American Ceramic Society 92 (2009) 763–780.
[19] E. Brightman, D.G. Ivey, D.J.L. Brett, N.P. Brandon, Journal of Power Sources 196 (2011) 7182–7187.
[20] C. Xu, P. Gansor, J.W. Zondlo, K. Sabolsky, E.M. Sabolsky, Journal of The Electrochemical Society 158 (2011) B1405–B1416.
[21] M. Chen, B.H. Kim, Q. Xu, B.G. Ahn, D.P. Huang, Solid State Ionics 181 (2010) 1119–1124.
[22] J.B. Goodenough, Y.-H. Huang, Journal of Power Sources 173 (2007) 1–10.
[23] C. Xia, M. Liu, Solid State Ionics 152–153 (2002) 423–430.
[24] L. Zhang, S.P. Jiang, H.Q. He, X. Chen, J. Ma, X.C. Song, International Journal of Hydrogen Energy 35 (2010) 12359–12368.
[25] B. Iwanschitz, J. Sfeir, A. Mai, M. Schutze, Journal of The Electrochemical Society 157 (2010) B269–B278.
[26] S. Primdahl, M. Mogensen, Solid State Ionics 152–153 (2002) 597–608.
[27] S. Primdahl, Y.L. Liu, Journal of The Electrochemical Society 149 (2002) A1466–A1472.
[28] J. Liu, B.D. Madsen, Z. Ji, S.A. Barnett, Electrochemical and Solid-State Letters 5 (2002) A122–A124.
[29] M.C. Tucker, G.Y. Lau, C.P. Jacobson, L.C. DeJonghe, S.J. Visco, Journal of Power Sources 171 (2007) 477–482.
[30] S.F. Corbin, X. Qiao, Journal of the American Ceramic Society 86 (2003) 401–406.
[31] T. Klemensø, K. Thydén, M. Chen, H.-J. Wang, Journal of Power Sources 195 (2010) 7295–7301.
[32] P.V. Aravind, J.P. Ouweltjes, J. Schoonman, Journal of The Electrochemical Society 156 (2009) B1417–B1422.
[33] J.C. Hirschfelder, C.F. Curtiss, R.B. Bird, Molecular Theory of Gases and Liquids, New York, 1954.
[34] W.C. Chueh, Y. Hao, W. Jung, S.M. Haile, Nature Materials 11 (2011) 155–161.
[35] A.J. Bard, L.R. Faulkner, Electrochemical Methods: Fundamentals and Applications, John Wiley & Sons, New York, 2001.
[36] T. Smith, Chemistry, University of Calgary, Calgary, 2007.
[37] T.S. Li, W.G. Wang, Journal of Power Sources 196 (2011) 2066–2069.